The Summertime Heat Budget and Circulation of Southeast New England Shelf Waters

JOHN L. WILKIN

Institute of Marine and Coastal Sciences, Rutgers, The State University of New Jersey, New Brunswick, New Jersey

(Manuscript received 22 December 2005, in final form 14 April 2006)

ABSTRACT

A modeling study of summer ocean circulation on the inner shelf south of Cape Cod, Massachusetts, has been conducted. The influences of winds, air–sea heat fluxes, tides, and shelfwide circulation are all incorporated. The model reproduces recognized features of the regional summer circulation: warm temperatures and weak eastward flow in Nantucket Sound, cool tidally mixed waters and an associated anticyclonic flow encircling the Nantucket Shoals, and strong stratification south of Martha's Vineyard. Comparisons with satellite and in situ observations show the model simulates the major features of the temperature patterns that develop during summer 2002. The evolution of the summer heat budget is characterized by three regimes: Nantucket Sound heats rapidly in June and then maintains warm temperatures with little net air–sea heat flux; tidal mixing on the Nantucket Shoals maintains perpetually cool ocean temperatures despite significant air–sea heating; and midshelf south of Martha's Vineyard the surface waters warm steadily through July and August because of sustained air–sea heating with only modest cooling resulting from the mean circulation. In the environs of the Martha's Vineyard Coastal Observatory tidal eddy heat flux emanating from Nantucket Sound produces a bowl of warm water trapped against the coast and significant local variability in the net role of advection in the heat budget. A suite of idealized simulations with forcing dynamics restricted, in turn, to only one of winds, tides, or shelfwide inflows shows that tidal dynamics dominate the regional circulation.

1. Introduction

The inner continental shelf of southeastern New England south of Cape Cod, Massachusetts, encompasses a variety of ocean circulation regimes delineated by the geography of the region (Fig. 1). The relatively shallow waters of Nantucket Sound are sheltered by the islands of Martha's Vineyard and Nantucket and experience the warmest summertime sea temperatures in the region (Limeburner and Beardsley 1982). Studies of the circulation within Nantucket Sound are few, but all indicate the mean flow is eastward during spring and summer (Bigelow 1927; Limeburner and Beardsley 1982). On the outer Cape Cod coast there is a southward flow of cool and relatively fresh waters exiting from the western Gulf of Maine. Though the majority of this transport turns eastward to circumnavigate Georges Bank, Limeburner and Beardsley (1982) estimate that some 15×10^3 m^3 s^{-1} inshore of the 30-m isobath continues southward through the Great South Channel along the eastern flank of the Nantucket Shoals, ultimately joining westward flow on the mid- to outer shelf. The Nantucket Shoals are vertically well mixed throughout the year, which it has been noted (Limeburner and Beardsley 1982; He and Wilkin 2006) is consistent with the h/U^3 tidal mixing process (Simpson and Hunter 1974), while the waters south of Martha's Vineyard undergo a seasonal cycle of stratification and mixing (Lentz et al. 2003). There is strong westward flow on the outer shelf in the shelf/slope front along approximately the 100-m isobath at the continental shelf break (Linder and Gawarkiewicz 1998).

This paper presents a modeling study of the heat budget of the inner shelf waters south of Cape Cod, with emphasis on the region south of Martha's Vineyard where observations were made during the summers of 2001, 2002, and 2003 as part of the low-wind-speed component of the Coupled Boundary Layers and Air Sea Transfer (CBLAST-Low) program (Edson et al. 2006). The CBLAST-Low study was centered on the Martha's Vineyard Coastal Observatory (MVCO) (Fig. 1) operated by the Woods Hole Oceanographic Insti-

Corresponding author address: John L. Wilkin, IMCS Rutgers, The State University of New Jersey, 71 Dudley Road, New Brunswick, NJ 08901.
E-mail: wilkin@marine.rutgers.edu

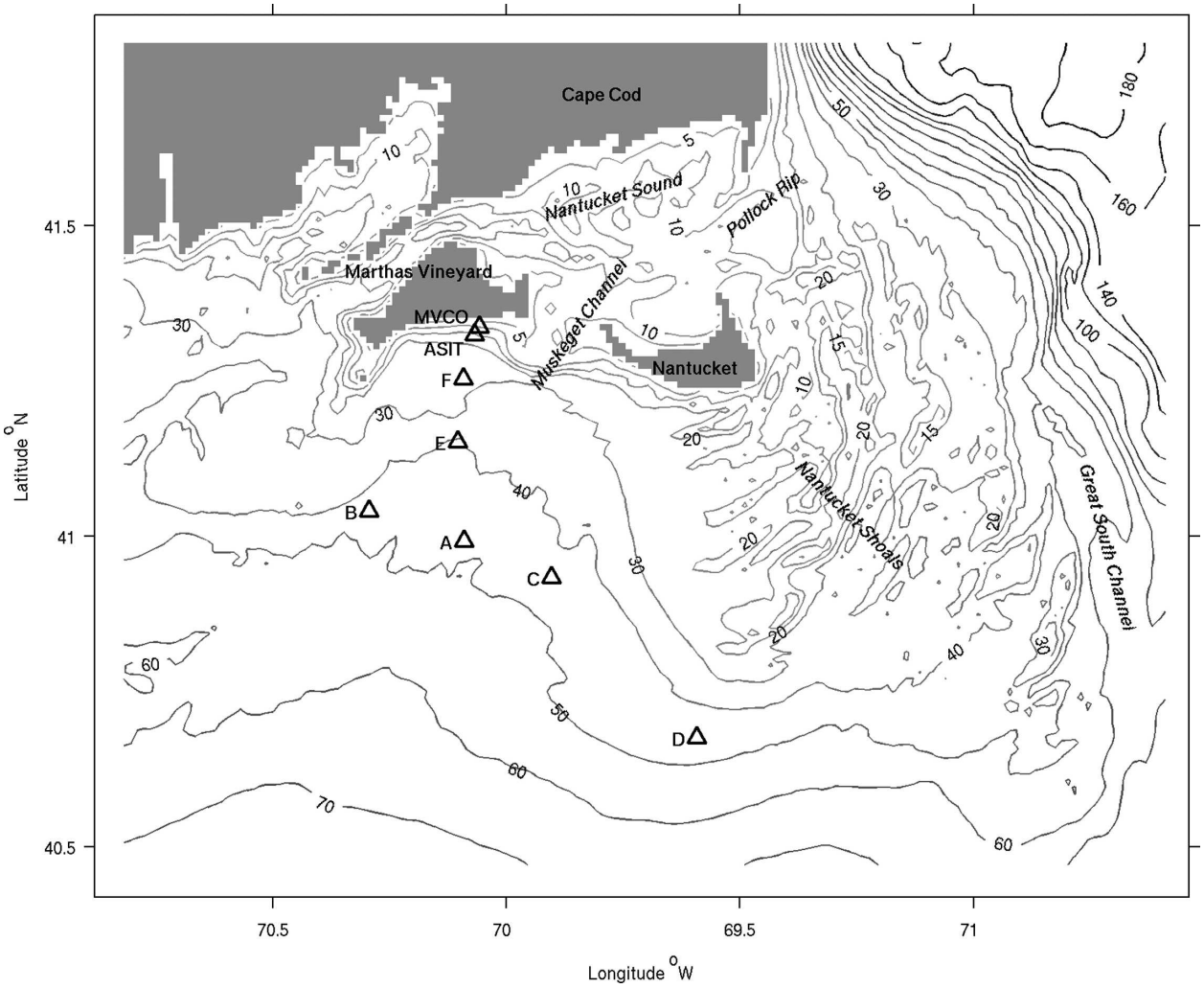

FIG. 1. Map of the study area showing the full ocean model domain, the model bathymetry (m), the site of MVCO and its associated Air–Sea Interaction Tower (ASIT), and the location of the 2002 CBLAST-Low moorings A–F.

tution. The observational program was designed to acquire turbulence and mean flow data from fixed towers and moorings in order to directly measure vertical fluxes of momentum and heat on both sides of the air–sea interface. These observations enable analysis of air–sea exchange and vertical mixing processes that are unresolved in atmosphere and ocean models and typically parameterized using vertical turbulence closure schemes and air–sea flux bulk formulas.

Lateral advection and mixing were largely unobserved by the CBLAST-Low network; yet, as will be shown, these processes are significant in the local heat budget at many locations throughout the region. Furthermore, under low wind conditions during summer, the oceanic mixed layer is often only a few meters thick and mesoscale oceanic circulation can potentially modulate the shallow mixed layer depth, thereby affecting sea surface temperature and air–sea fluxes. It is therefore important to consider the vertical flux observations within a regional spatial context of mesoscale variability.

The ocean model has been configured with a high level of realism in order to examine the mesoscale response of inner shelf waters in this region to tides, local meteorology, and shelfwide external forcing, and to provide support for the interpretation of CBLAST-Low mooring observations. The modeling objective is to capture the essential features of the three-dimensional ocean heat transport on diurnal to several day time scales, and spatial scales of order 1 km. In summer 2002, seven moorings gathered surface meteorological data and subsurface temperature and velocity profiles in an across- and along-shelf pattern south of Martha's Vineyard (Hutto et al. 2003) (Fig. 1). In concert with

observations from the MVCO site, these provide the data against which the skill of the model is evaluated.

The ocean model configuration is described in section 2. Comparisons of the simulations with observations are shown in section 3. The relative roles of meteorology, tides, and open boundary influences in the dynamics are presented in section 4, and this understanding is used to interpret the modeled heat budget in section 5. Implications for the interpretation of CBLAST-Low observations and the overall role of mesoscale ocean circulation in modulating lateral heat transport, mixed layer depth, and air–sea fluxes in the region are discussed in section 6.

2. The regional ocean model

The ocean simulations presented here were performed using the Regional Ocean Modeling System (ROMS; http://marine.rutgers.edu/roms), a free-surface, hydrostatic, primitive equation model in widespread use for estuarine, coastal, and shelfwide applications (MacCready and Geyer 2001; Dinniman et al. 2003; Lutjeharms et al. 2003; Marchesiello et al. 2003; Peliz et al. 2003; Warner et al. 2005; Wilkin et al. 2005). ROMS employs the split-explicit separation of barotropic and baroclinic modes, and is formulated in vertically stretched terrain-following coordinates using algorithms described in detail by Shchepetkin and McWilliams (1998, 2003, 2005). The ROMS computational kernel includes high-order advection and time-stepping schemes, weighted temporal averaging of the barotropic mode to reduce aliasing into the baroclinic motions, and a redefinition of the barotropic pressure-gradient terms to account for local variations in density field to significantly reduce the pressure-gradient truncation error that has previously limited the accuracy of terrain-following coordinate models. Vertical discretization uses conservative parabolic splines.

a. Model configuration

The model domain is centered on the CBLAST-Low observation area, and extends west–east from Narragansett Bay to the saddle of the Great South Channel, and north–south from Cape Cod to just beyond the 60-m isobath at 40°30′N (Fig. 1). The southern open boundary is well within the typical summertime location of the shelf/slope front (Linder and Gawarkiewicz 1998; Lentz et al. 2003) so that open boundary influences are dominated by inflow from the Gulf of Maine.

Horizontal grid resolution is 1 km. There are 20 vertical levels weighted toward the sea surface such that in 30 m of water the grid resolution in the surface mixed layer is 0.5 m. The model bathymetry is interpolated from the National Geophysical Data Center (NGDC) Coastal Relief Model (Divins and Metzger 2003) augmented by soundings digitized from charts in Muskeget Channel. Open boundary conditions are applied to tracers and baroclinic velocity using Orlanski-type radiation conditions in conjunction with relaxation (Marchesiello et al. 2001), with time scales of 0.5 days on inflow and 10 days on outflow, to a regional bimonthly climatology (Naimie et al. 1994). The free surface and depth-integrated velocity boundary conditions use the method of Flather (1976) with external values specified as the climatology plus tidal harmonic variability from an Advanced Circulation (ADCIRC) model simulation of the western Atlantic (Luettich et al. 1992) tuned to match local observations of bottom pressure in the CBLAST-Low region (He and Wilkin 2006). Quadratic bottom drag and vertical turbulent mixing using the method of Mellor and Yamada (1982) complete the model configuration.

b. Surface forcing

Starting from June climatological conditions (Naimie et al. 1994), hindcast simulations were made for June through September 2002 using atmospheric forcing from a high-resolution (3-km horizontal grid at the innermost nest) Coupled Ocean/Atmosphere Mesoscale Prediction System (COAMPS) (Hodur et al. 2002) meteorological forecast that was run operationally to provide information to field scientists during the CBLAST-Low Intensive Operating Period (Wang et al. 2004). Air–sea fluxes of momentum and sensible, latent, and longwave heat are computed by applying bulk formulas (Fairall et al. 2003) to COAMPS marine boundary layer winds, temperature, humidity, and pressure, and ROMS sea surface temperature (SST) and current.

The archived COAMPS data for 2002 do not fully capture the shortwave radiation diurnal cycle, or separate longwave radiation into atmospheric downward and oceanic upward contributions. To accurately represent diurnal heating and to allow the modeled ocean SST to enter in the net longwave radiation calculation, the ocean model is forced with downward shortwave and longwave radiation from hourly observations from mooring A (Fig. 1). Radiometer data from the six surface moorings are highly correlated (Hutto et al. 2003) so observations from mooring A are characteristic of the CBLAST-Low region, and there is little to indicate that the loss of spatially resolved downward radiation will limit the model skill.

To check whether meteorological conditions in 2002 might be anomalous, statistics of July average surface air temperature, humidity, and wind speed from Na-

tional Centers for Environmental Prediction (NCEP) reanalysis data for 1979 through 2005 were analyzed. The July 2002 values fell well within one standard deviation of the 27-yr mean, so it is expected that the characteristics of the modeled circulation should be typical of summer conditions.

3. Comparisons of model and observations

The modeled temperature and currents at 2-m depth, averaged for the months of July and August 2002, are shown in Fig. 2. Several qualitative features of the regional circulation described previously are evident; namely, the warmest temperatures and weak eastward flow in Nantucket Sound, southward transport of cool waters from the outer Cape southward through the Great South Channel, and westward flow in the south that encircles the Nantucket Shoals. The coolest temperatures occur over steep bathymetry southeast of Pollock Rip Channel.

A tongue of warm water issues from Nantucket Sound through Muskeget Channel and encroaches on MVCO but is opposed by the local mean flow, indicating that an eddy flux of heat likely sustains the adverse temperature gradient. This eddy flux is the consequence of pulses of warm water that exit Nantucket Sound on each ebb tide. The process is depicted in Fig. 3, which shows the temperature at 5-m depth at approximately 2-h intervals during a period of low winds on 3 August 2002. This heat transport forms a region of warm water trapped against the south coast of Martha's Vineyard that can be seen in north–south vertical sections (Fig. 4) from the coast to mooring E. There were no synoptic CTD surveys of the region during 2002 to directly substantiate the occurrence of the warm-water bowl in the simulation, but it is a robust feature of summertime conditions observed in CTD transects during the 2001 and 2003 CBLAST-Low studies (Pritchard et al. 2002; Hutto et al. 2005) and by autonomous underwater vehicles in 2002 [K. Shearman 2004, personal communication; Remote Environmental Measuring Units (REMUS) autonomous underwater vehicle (AUV) data] and 2003 (Fig. 4d). CTD data from 23 July 2001 during the CBLAST pilot experiment (Fig. 4c) may be compared with model results (Fig. 4a) for the corresponding yearday in 2002. Similarly, Figs. 4b and 4d compare model output for 19 August 2002 and temperature observations from a Webb Research Corporation coastal glider (O. Schofield 2004, personal communication) acquired over the 3 days 18–21 August 2003. In the August comparison, model and data show similar slopes in the thermocline as it deepens toward the Martha's Vineyard coast, though the thermocline itself is more diffuse in the model. Both sets of observations show a bowl shape to the thermocline close to the coast, consistent with the weak anticyclonic sense to the modeled circulation in the region shown in Fig. 2.

Figure 5 shows the time series of temperature at mooring F (the closest to MVCO of the five moorings deployed in 2002) and the corresponding time series modeled by ROMS. The model captures the dominant features of the evolving thermal stratification. The water column is weakly stratified in early summer, becoming strongly stratified in the beginning of July. There is a cool bias in the model temperatures at the beginning of July, possibly associated with model initial conditions, but this is largely eliminated by mid-July. A cooling event near the end of July appears in the model 1.5 days too early, but thereafter the model and observations are in clear agreement. The late July cooling event is due to a meandering cold front briefly moving across the mooring location, with imprecision in the simulated timing likely due to short wavelength submesoscale variability along the slowly moving frontal boundary.

The overall skill of the simulation may be quantified in terms of the mean-squared error between model and mooring observations, $\mathrm{MSE} = \langle (m_i - o_i)^2 \rangle$, where m_i and o_i are the ith modeled and observed values, respectively, and the angle brackets denote a mean over the time series. MSE is one of many possible quantitative measures of model skill. Oke et al. (2002) show that MSE comprises contributions from the mean bias, $\mathrm{MB} = \langle m \rangle - \langle o \rangle$, the standard deviation error, $\mathrm{SDE} = S_m - S_o$, and the cross-correlation, $\mathrm{CC} = S_m^{-1} S_o^{-1} \langle (m_i - \langle m \rangle)(o_i - \langle o \rangle) \rangle$:

$$\mathrm{MSE} = \mathrm{MB}^2 + \mathrm{SDE}^2 + 2S_m S_o (1 - \mathrm{CC}), \qquad (1)$$

where S_m and S_o are the respective model and observed standard deviations. Vertical profiles of the three contributions to the error and the square root of MSE (RMSE) for mooring F are plotted in Fig. 6. The mean bias is small, but shows the model to be slightly too cool at the surface and too warm at depth. RMSE is around 1.5°C at all depths and due in near-equal proportions to the standard deviation and cross-correlation terms.

Of the six mooring locations, site F is where the model is most skillful. Figure 7 compares these error terms for all moorings. At sites B, A, and C along the 45-m isobath south of Martha's Vineyard the model shows similar performance, being about 2°C cool near the surface and biased warm by a similar amount at depth. Near the seafloor the bias is smaller. Averaged over depth the mean bias ranges in magnitude from 0.07° (mooring F) to 1.3°C (mooring E) with a mean over all moorings of 0.6°C. To put this temperature error in perspective, it corresponds to an error in heating over the two months of the model–data comparison

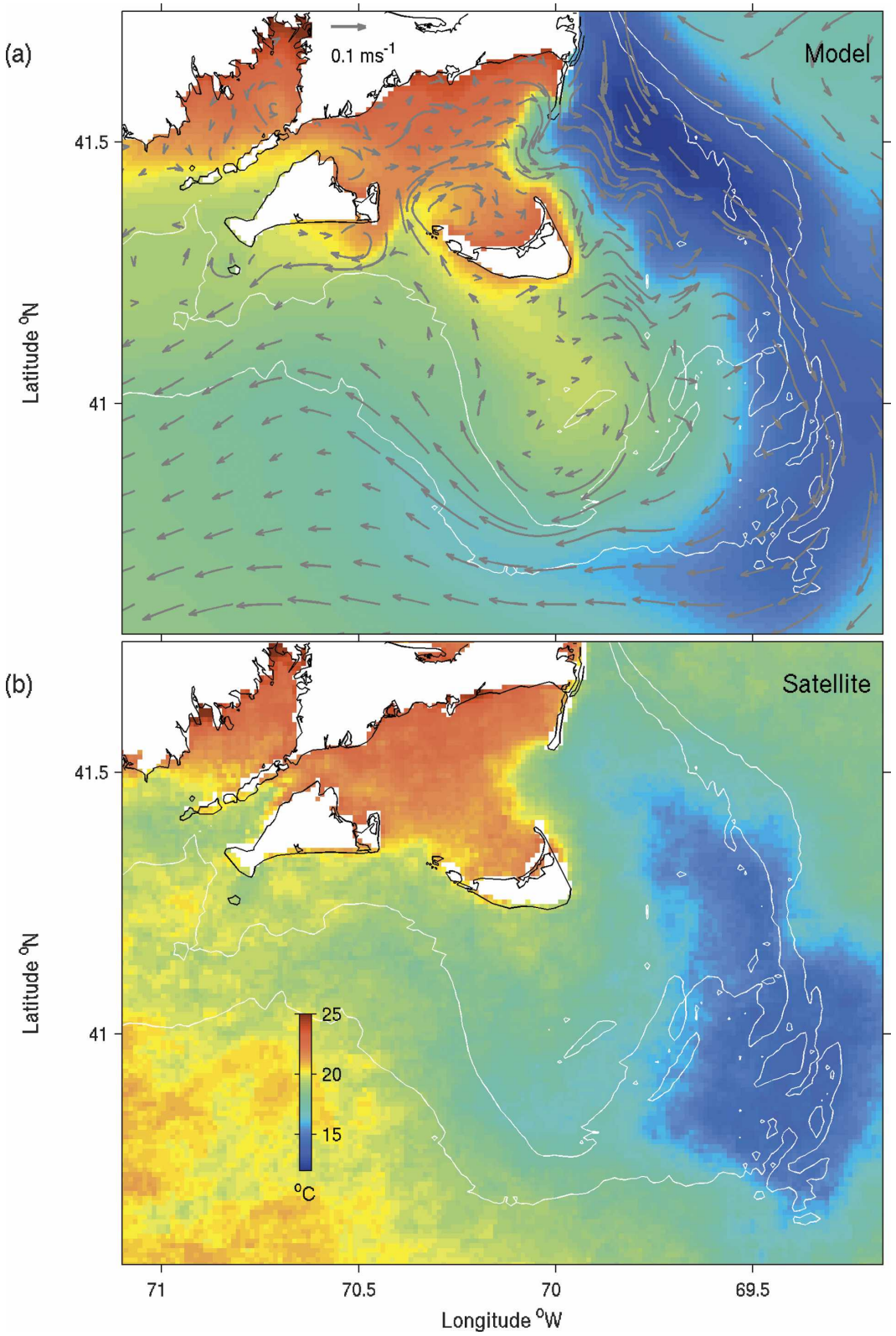

FIG. 2. Mean surface temperature in July and August 2002. (a) Modeled. Arrows show mean current at 2-m depth. (b) Satellite sea surface temperature. Gray lines show 30- and 45-m isobaths.

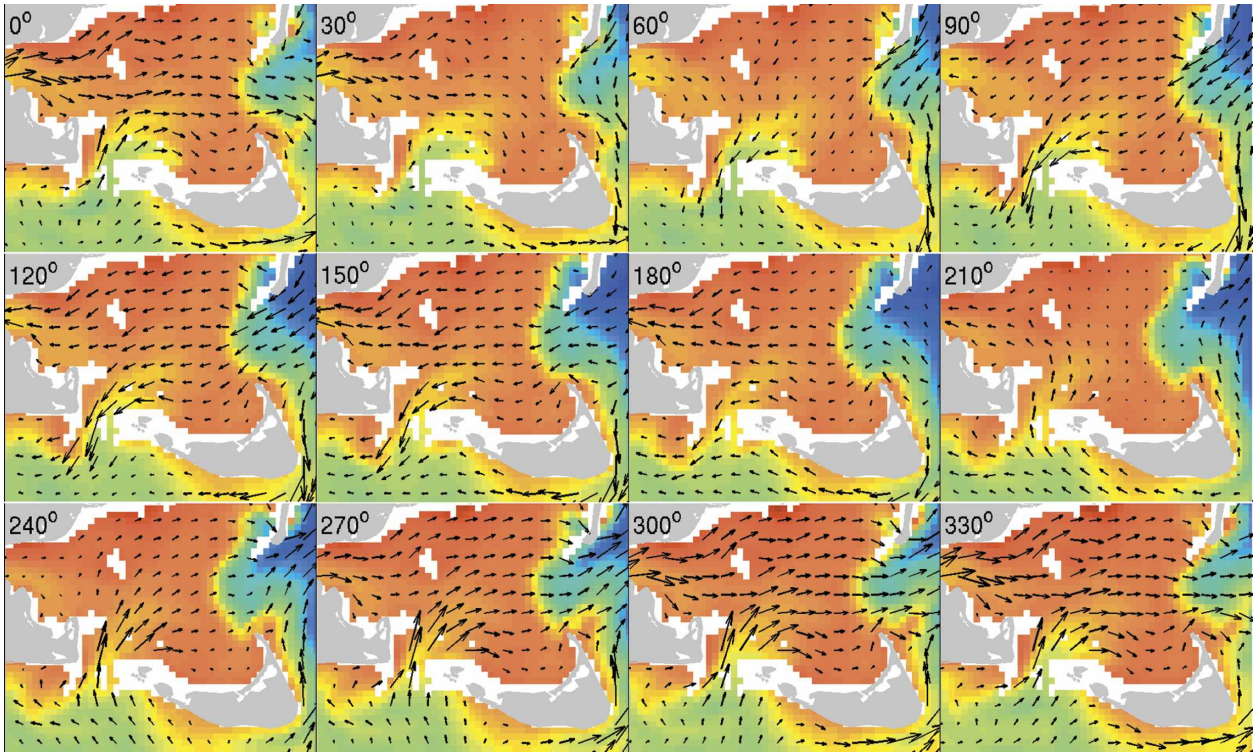

FIG. 3. Temperature and velocity at 5-m depth in Nantucket Sound through a tidal cycle during low wind conditions on 3 Aug 2002. The phase of the M_2 tide in degrees is given relative to the beginning of the ebb at Pollock Rip. These figures may be compared with the current charts for Nantucket Sound in Eldridge (2005). The ebb tide carries warm Nantucket Sound water through Muskeget Channel and toward MVCO.

of just 16 W m^{-2}, showing the net heat content is roughly correct. The surface cool bias and deeper warm bias suggest the model does not evolve sufficiently strong stratification during the summer. There is very little deep bias at mooring D nearest to Nantucket Shoals where tidal mixing entrains cold waters at depth, but the modeled surface temperatures are still too cool. At moorings A–D, negative SDE peaks at 10–15-m depth revealing that model variance there is too low. This is the typical depth of the mixed layer throughout July and August (Hutto et al. 2003) suggesting the modeled thermocline depth does not fluctuate sufficiently, or that the temperature contrast across the thermocline is too small (which would be consistent with the mean bias). Similarly, the magnitude of the cross-correlation term peaks at this depth. The combined RMSE at moorings A–D is greatest at mid-water-column depth below the mixed layer, and takes a local minimum above the base of the mixed layer where the mean bias happens to be near zero. Mooring E, located midway between the 45-m isobath and inner mooring F due south from MVCO, has smaller errors than the outer moorings but not as low as mooring F itself. Thus there is a trend toward generally higher model skill closer to MVCO, the region of principal interest in this study. The cross correlation (which excludes the effect of mean bias) between modeled and observed variability is high at moorings E and F (Fig. 7e) with vertically averaged values of 0.62 and 0.77, respectively.

A quantitative measure of predictive skill (Wilmott 1981) recently used to evaluate ROMS in a simulation of the Hudson River (Warner et al. 2005) is

$$\text{Skill} = 1 - \frac{\text{MSE}}{\langle (|m_i - \langle o \rangle| + |o_i - \langle o \rangle|)^2 \rangle}. \qquad (2)$$

Perfect agreement of model with observations would return a skill of 1. This skill is plotted in Fig. 7f. The same trends noted above are evident; principally, that the model is most skillful at mooring F, where the vertical average Skill indicates the model captures 77% of the temperature variability, but this decreases moving southward to 62% at mooring E and 46%, 49%, and 55% at the outer moorings A, B, and C, respectively.

The model–data comparison above shows that the model has useful skill at reproducing observed temperature variability, especially closest to MVCO in the area of principal interest to the air–sea exchange inten-

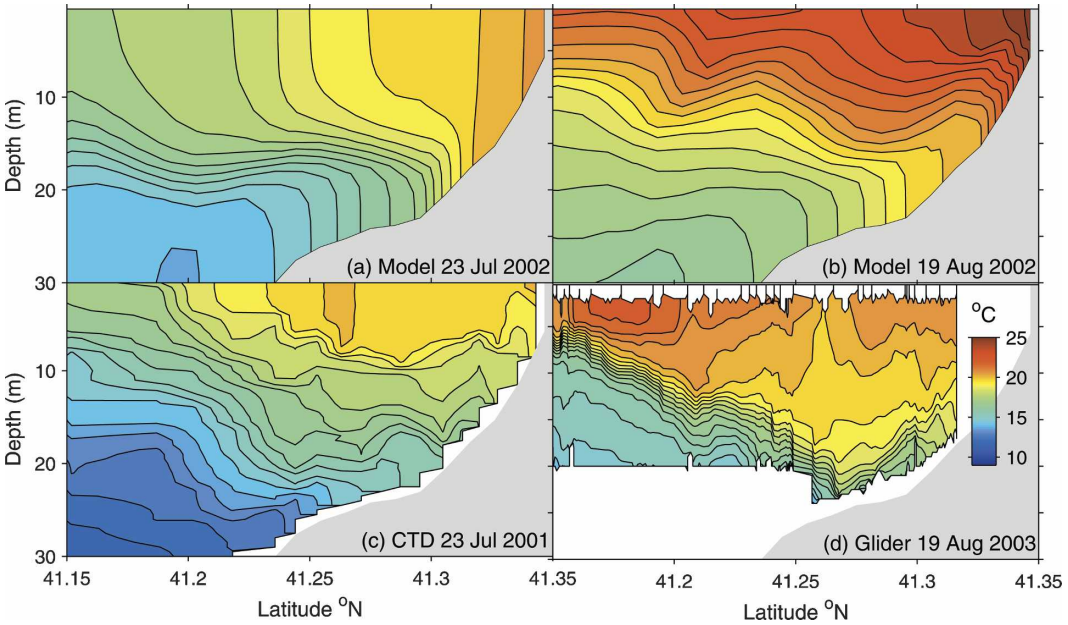

FIG. 4. Vertical sections of temperature along 70°34′W from the Martha's Vineyard coast to mooring E. (a) Model, 23 Jul 2001. (b) Model, 19 Aug 2003. (c) CTD observations on 23 Jul 2001. (d) Webb Research Corporation glider-type AUV observations acquired from 18 to 21 Aug 2003.

sive observations. This skill and the qualitative simulation of recognized mean circulation patterns indicate that the model has met the objective of reproducing the dominant features of the summertime thermal variability. The dynamical processes that influence the heat budget in the region are considered next.

4. Dynamics: Tides, meteorology, and shelfwide forcing

Features of the barotropic tidal dynamics in this region were analyzed by He and Wilkin (2006). These features include a significant tidal residual mean circulation clockwise around the Nantucket Shoals and, more importantly for the regional heat budget, indications that tidal stirring over much of the shoals is expected to be sufficiently strong to vertically mix the water column despite the strong buoyancy input from summertime solar heating. Where the balance of these two processes tips there can form a tidal mixing front (Simpson and Hunter 1974; Simpson et al. 1978) between the well-mixed and stratified regimes. For the European shelf seas, Simpson and Hunter (1974) pre-

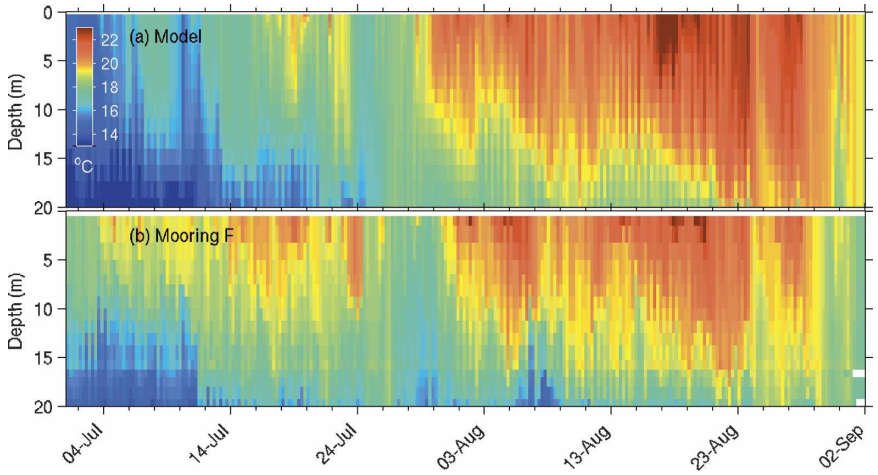

FIG. 5. Time series of vertical temperature profile at the mooring F site. (a) Observed. (b) Modeled.

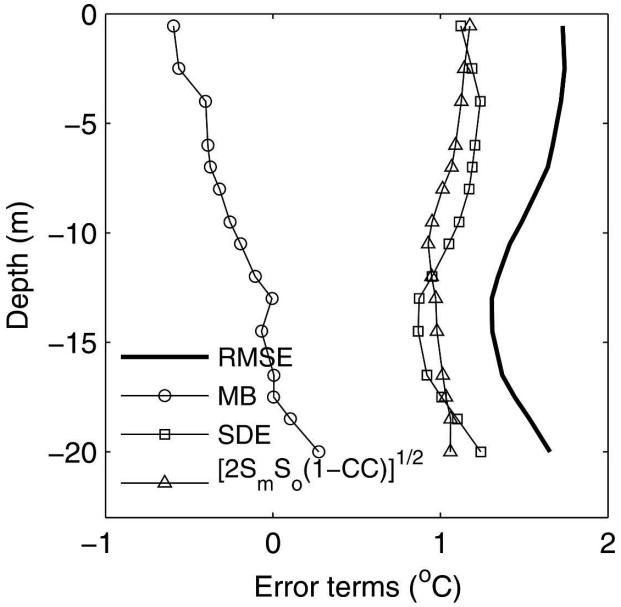

FIG. 6. Vertical profiles of terms in Eq. (1) contributing to the RMSE at mooring F. Terms are mean bias (MB), standard deviation error (SDE), and cross-correlation error $[2S_mS_o(1 - CC)]^{1/2}$, all in °C.

dict that tidal mixing fronts form near a critical value of $\log_{10}(h/U^3) = 2.7 \pm 0.3$, where h is the water depth (meters) and U is the magnitude of the depth-average tidal current (meters per second). Whereas the homogeneous (constant density) model used by He and Wilkin (2006) could infer only the likely location of mixing fronts, with the present model the simulated stratification can be compared directly with velocity variability. Estimating U as the standard deviation over all time scales, rather than solely from the tides, contours of $\log_{10}(h/U^3)$ are plotted in Fig. 8a over a map of the summer mean surface to bottom density gradient, $(\rho_{z=-h} - \rho_{\text{surface}})/h$. The 2.7 contour somewhat overestimates the extent of the zone of low vertical stratification, and the value 2.4 better delineates the region. A vertical section of mean density along 41.1°N (Fig. 8b) confirms that the region of weak stratification largely coincides with the lower 2.4 criterion.

Tidal stirring clearly influences vertical mixing and stratification, and therefore likely affects the regional heat budget. To examine how significant the tides are relative to other processes, a set of model simulations were conducted to isolate the dynamic influences on

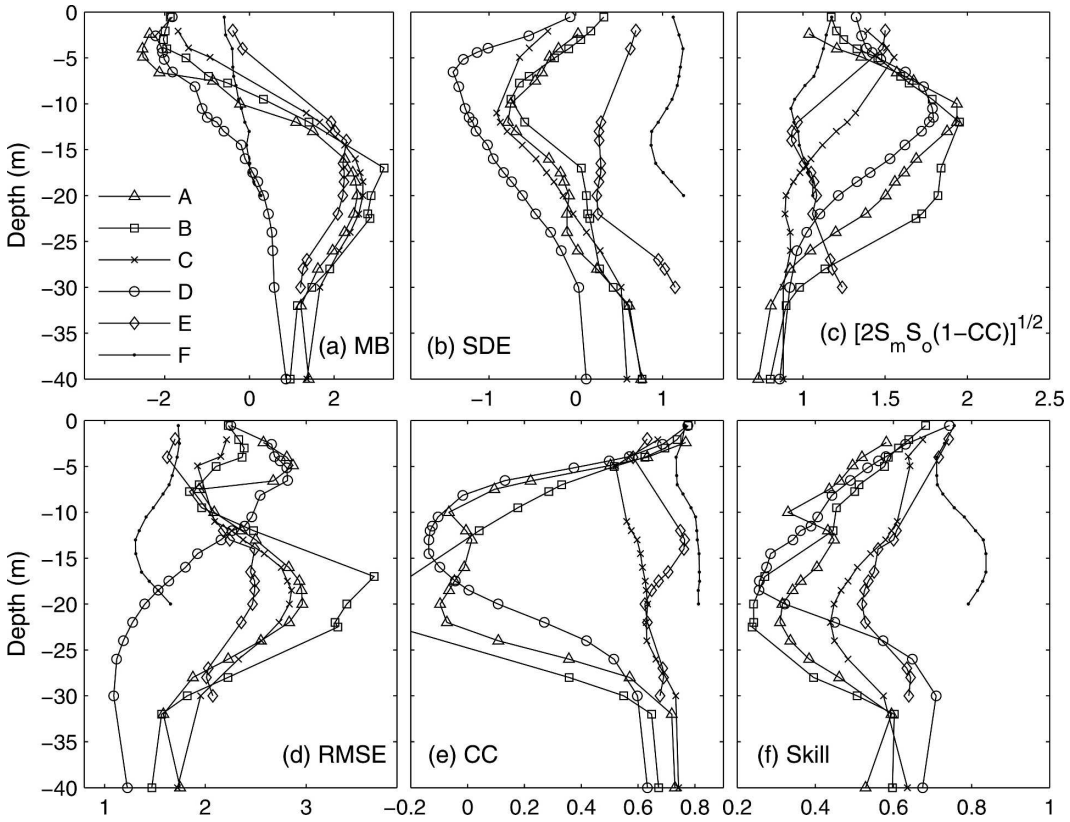

FIG. 7. Vertical profiles of model-data error terms for all CBLAST 2002 moorings A–F. (a)–(d) The same error terms plotted in Fig. 6. (e) Cross-correlation, which shows the model-data agreement when the effect of mean bias is excluded. (f) Skill score (Wilmott 1981).

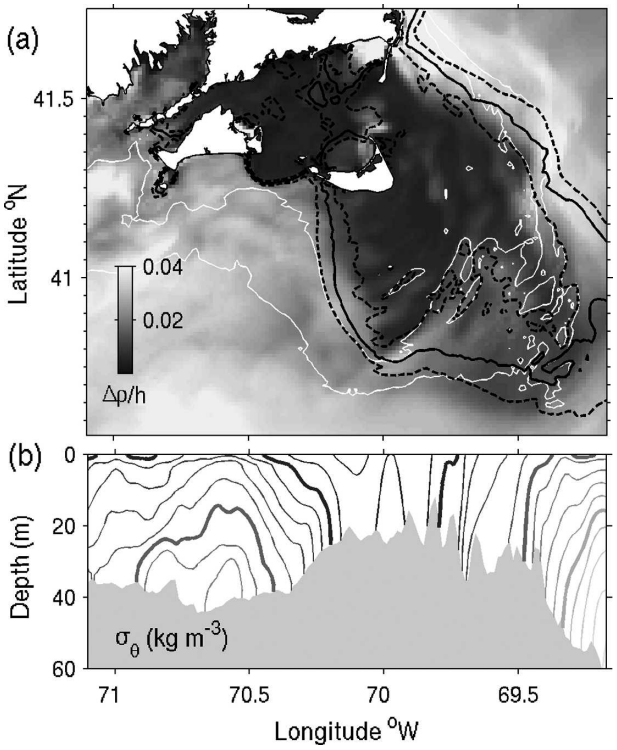

FIG. 8. (a) Mean July–August stratification (kg m^{-4}) computed as the surface to bottom density gradient $(\rho_{z=-h} - \rho_{\text{surface}})/h$. Dark contours show $\log_{10}(h/U^3)$, where U is the std dev of depth-averaged velocity. Solid dark contour is the value 2.7 that Simpson et al. (1978) observe defines the boundary of vertically tidally stirred regions in the European shelf seas. Dashed dark contours are 2.4 and 3.0. White contours are the 30- and 45-m isobaths. (b) Section of mean density (σ_θ) along 41.1°N. Contour interval is 0.2 kg m^{-3}. Heavy contours are 23, 24, and 25 kg m^{-3}.

the circulation of tides, winds, and open boundary forcing.

Using the same basic model configuration, three further simulations of the June–August period were conducted. In an experiment denoted *wind only*, the observed 2002 winds were applied as before, but boundary tides were omitted and the initial and open boundary climatology conditions were replaced with horizontally uniform vertical profiles of temperature and salinity; that is, the stratification is strictly vertical so that neither initial nor boundary conditions impose a thermal wind or barotropic pressure gradient. In an experiment denoted *climatology only*, the winds and boundary tides were set to zero, but the original initial conditions and open boundary climatology that impose a shelfwide baroclinic and barotropic pressure gradient were retained. In an experiment denoted *tide only*, tides were retained but the winds were zero and the initial and boundary stratification again functions of z only. The *tide only* experiment is therefore similar to the model of He and Wilkin (2006) but with the inclusion of initial stratification.

The summertime winds are upwelling favorable and drive eastward flow both through Nantucket Sound and along the southeast coast of the island itself (Figs. 9a,b, *wind only*). It should be noted that this simulation is for summer forcing only, and that the prevailing northeast winds in winter will induce a different response. There is also eastward flow across a broad band to the south of Martha's Vineyard around 41°N, where tides drive a much stronger opposing westward mean current that branches from the tidal residual anticyclonic flow encircling the Nantucket Shoals (Fig. 9c,d, tide only). At the southeast corner of Martha's Vineyard there is a pronounced tidal residual anticyclonic eddy. In the absence of winds and tides, the externally imposed shelfwide pressure gradient drives circulation confined mostly to deeper waters (Fig. 9e, *climatology only*). In the Great South Channel this flow is in the same sense as the tide only circulation, but is not entirely independent because the climatology (Naimie et al. 1994) includes the net influence of tides. However, without local tidal mixing the shelfwide forcing alone does not drive the flow seen in the tide only case that follows shallower isobaths due south of Muskeget Channel and advances toward the MVCO region. The climatological open boundary forcing evidently contributes to the eastward mean flow in Nantucket Sound (Fig. 9f). The mean circulation with all forcing terms included (Fig. 2) shows that the tidally driven mean flow prevails over the winds south of the MVCO region.

The vector sum of the depth-average velocity in the three individual forcing scenarios is in close agreement with the mean circulation in the full forcing case, indicating that the three processes act largely independently. The ratio of combined depth-average velocity to the full forcing result has a mean value of 1.25, which is consistent with the net effect of quadratic bottom drag being underestimated when the bottom velocity is split into three smaller contributions.

5. Regional heat budget

Winds, tides, and open boundary influences all act to affect horizontal circulation and stratification in the model domain, so it is to be anticipated that there could be significant lateral transports of heat in the region. This is confirmed by separating the depth-integrated heat budget into its three contributions: storage (dT/dt), net air–sea flux (Q_{net}), and horizontal divergence ($-\nabla \cdot \mathbf{u}T$), averaged for the month of July (Fig. 10). The mean air–sea heat flux (Fig. 10a) is greatest east of Nantucket Sound in the region of consistently cool SST

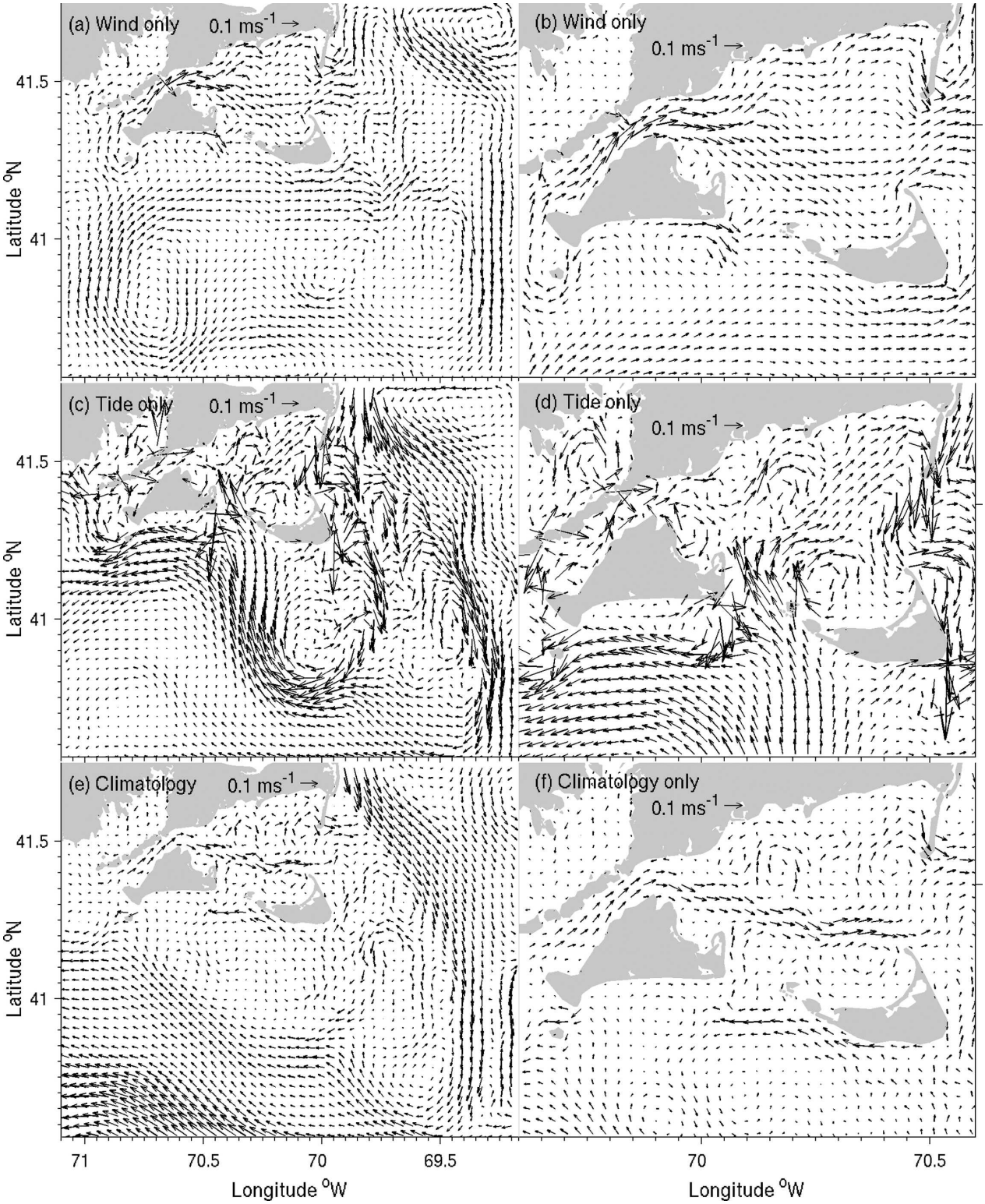

FIG. 9. July–August depth-averaged mean currents for the three idealized forcing scenarios described in the text. (a), (b) Wind only, (c), (d) tide only, (e), (f) boundary climatology only. (left) Vectors at every third model grid point. (right) Enlarged views of the left panels to more clearly show the circulation around the islands, with vectors plotted every second grid point.

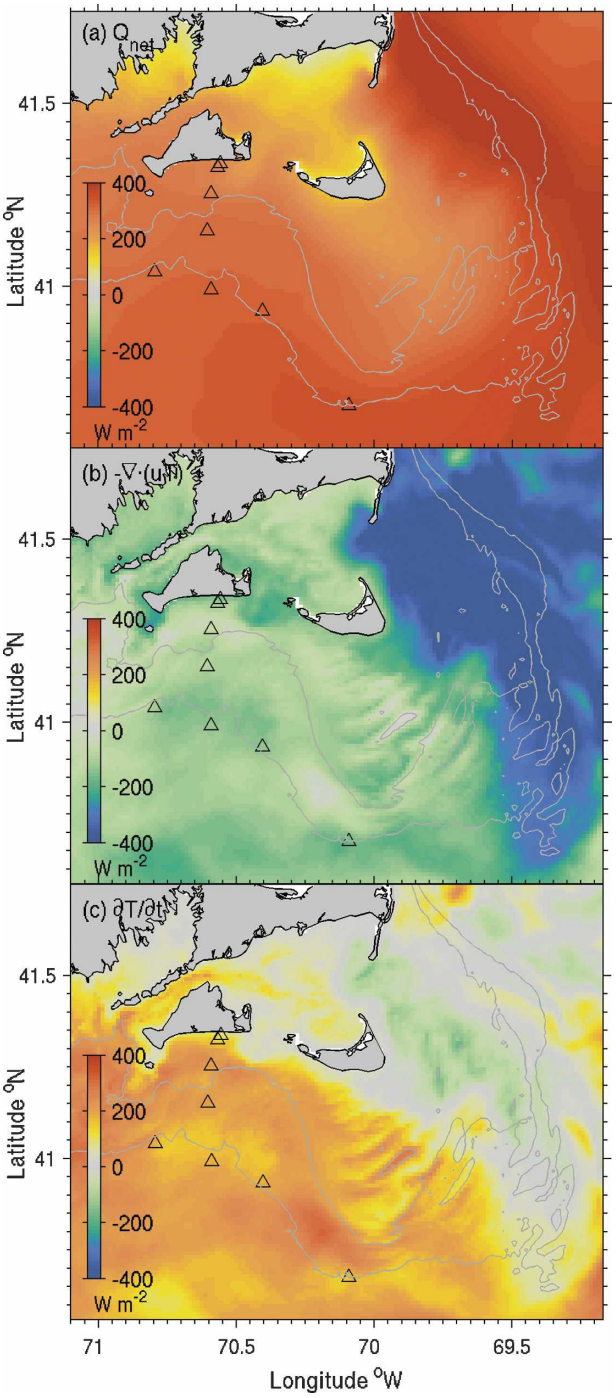

FIG. 10. July 2002 average of the three terms in the depth-integrated heat budget: (a) net air–sea flux (Q_{net}), (b) horizontal divergence ($-\nabla \cdot \mathbf{u}T$), and (c) storage ($dT/dt$). Sign convention for (a) and (b) is that positive causes warming.

(see Fig. 2), and is balanced by horizontal divergence (Fig. 10b); the substantial net heating from solar input and the air–sea temperature difference is exported laterally into the adjacent stratified regions by horizontal tidal mixing. When other months are considered this balance is seen throughout the summer. The rate of heat storage is also small within Nantucket Sound because the water has reached its summertime equilibrium (the heating rate in the Sound is greatest during June; not shown). The warm surface temperatures in the sound foster greater heat loss due to latent heat (85 W m^{-2}) and net longwave radiation (31 W m^{-2}) than occurs elsewhere in the model domain, leading to the smaller net air–sea warming in the sound (130 W m^{-2}; Fig. 10a). The patterns of latent and longwave heat exchange mimic SST. Sensible heat exchange is small—less than 10 W m^{-2} almost everywhere.

There is a significant warming trend in a broad area south of the islands and west of the shoals indicating the region is still responding to summertime heating during July. South of Nantucket $\nabla \cdot \mathbf{u}T$ is low in magnitude in a localized band extending northwestward from mooring D on the outer shoals, generally confined between the 30- and 45-m isobaths. Surface heat flux in this band therefore leads to a direct increase in heat content, suggesting the heating process is locally one-dimensional in the vertical. This is not, however, because currents are weak; near-surface velocity in the region is some 0.3 m s^{-1} (Fig. 2). So while horizontal currents are substantial, evidently this does not lead to a divergence of heat. The observed and modeled mean SST (Fig. 2) show this zone coincides with a tongue of cool water drawn from the cold tidally mixed Nantucket Shoals. Water teased out from the cold patch joins the tidally rectified mean flow directed to the northwest. Once out of the sustained cooling influence of tidal mixing these waters progress northwestward warming and restratifying because of heating at the surface with little gain or loss of heat from the surrounding waters.

Along the south coast of Martha's Vineyard the net $\nabla \cdot \mathbf{u}T$ term is significant in the local heat balance, acting to cool the water column. Near MVCO the July air–sea heat flux is about 250 W m^{-2}, of which only 100 W m^{-2} goes to warming the water column while the other 150 W m^{-2} (cooling) is removed by the circulation. The contributions over time of air–sea flux and advection to the net heat storage at the model grid point nearest to MVCO are shown in Fig. 11 in terms of the equivalent heating in degrees Celsius. This emphasizes that the water column warms much less rapidly than expected from the air–sea heat input alone. The high-frequency variability is related to the tidal pulses of heat associated with the flow through Muskeget Channel that was noted in section 3, and will be discussed further below.

To the south of MVCO, inside the 30-m isobath and close to mooring F, the magnitude of $\nabla \cdot \mathbf{u}T$ is less (Fig.

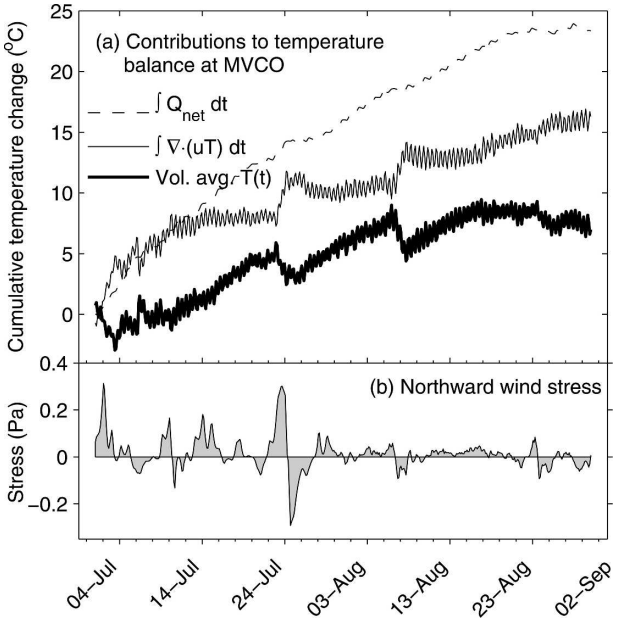

FIG. 11. (a) Time integral of vertically averaged terms in the temperature balance centered on the Martha's Vineyard Coastal Observatory. All terms are expressed as equivalent cumulative temperature change (°C). Dashed line: air–sea heating $\int_0^t (\rho c_p h)^{-1} Q_{\text{net}}\, dt'$. Light solid line: horizontal divergence $\int_o^t h^{-1} \int_{-h}^{0} \nabla \cdot (\mathbf{u}T)\, dz\, dt'$. Heavy solid line: net temperature change $\int_o^t h^{-1} \int_{-h}^{0} \partial T/\partial t\, dz\, dt'$; h is the water depth. (b) Northward component of wind stress at MVCO. See Fig. 12b for the eastward wind stress (the winds at MVCO and mooring F are highly correlated).

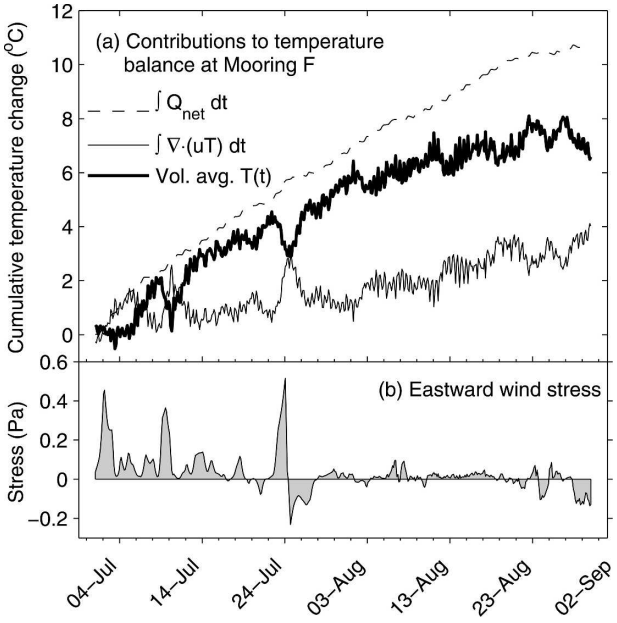

FIG. 12. (a) As in Fig. 11a but for the model grid point closest to mooring F. (b) Eastward wind stress at mooring F.

10). Figure 12 shows the time integral of the heat budget terms for the model grid point nearest to mooring F. Here, the temperature gain more closely follows the air–sea heating, showing a less significant role played by net advection. However, this is a not a region of weak currents or homogenous temperature.

For the MVCO and mooring F locations, the July averaged net advection of heat into a 3 km × 3 km control volume, $\rho c_p \int_V \nabla \cdot \langle \mathbf{u}T \rangle\, dV$, has been separated into contributions from the steady flow, $\int_V \nabla \cdot \langle \mathbf{u} \rangle \langle T \rangle\, dV$, and eddy variability, $\int_V \nabla \cdot \langle \mathbf{u}'T' \rangle\, dV$, where angle brackets denote the July mean over 60 M_2 tidal periods and primes denote the departure therefrom; ρc_p is the product of density and specific heat of seawater. It is found that steady advection cools the MVCO volume at 347 W m^{-2}, while the eddy heat flux (which is dominated by tidal variability) warms the location at 195 W m^{-2}, for a net cooling of 152 W m^{-2}. The net contribution of advection at the mooring F site is a more modest 66 W m^{-2} because there is more of a balance between steady flow and eddy transports of heat; the steady circulation cools the mooring F box at 211 W m^{-2} whereas the eddy transport warms the location at 145 W m^{-2}.

Figure 13 shows the steady flow and eddy contributions to the depth-integrated heat budget in this region in more detail. Vectors of eddy temperature flux $\langle \mathbf{u}'T' \rangle$ are formed from the residual of $\langle \mathbf{u}T \rangle$ minus the steady circulation temperature flux $\langle \mathbf{u} \rangle \langle T - T_o \rangle$, where T_o = 18°C is an approximate mean temperature in the region. Temperature fluxes are computed with reference to a local mean so that the direction of the vectors corresponds to the sense of heat transport. The eddy flux and steady flow vectors in Figs. 13a and 13b, respectively, are plotted over their divergence, which removes the ambiguity of reference temperature by virtue of continuity (because $T_o \boldsymbol{\nabla} \cdot \langle \mathbf{u} \rangle = 0$). Eddy temperature flux vectors diverge where the flow emanates from Muskeget Channel causing local cooling (dark shading) of the water column. Subsequent convergence deposits this heat in two zones just east of MVCO and mooring F. This is the process, described in section 3, whereby the exit of warm waters from Nantucket Sound on each ebb tide produces the bowl of warm water adjacent to the southeast Martha's Vineyard coast. The steady circulation (i.e., mean flow advecting the mean temperature) (Fig. 13b) compensates by removing somewhat more heat to produce the net cooling effect noted above.

Figures 11 and 12 show a few notable cooling episodes that briefly reverse the steady summer warming trend. In both time series sudden cooling on 24 July is associated with strong southwesterly upwelling favorable winds that bring in cool water from the west. A

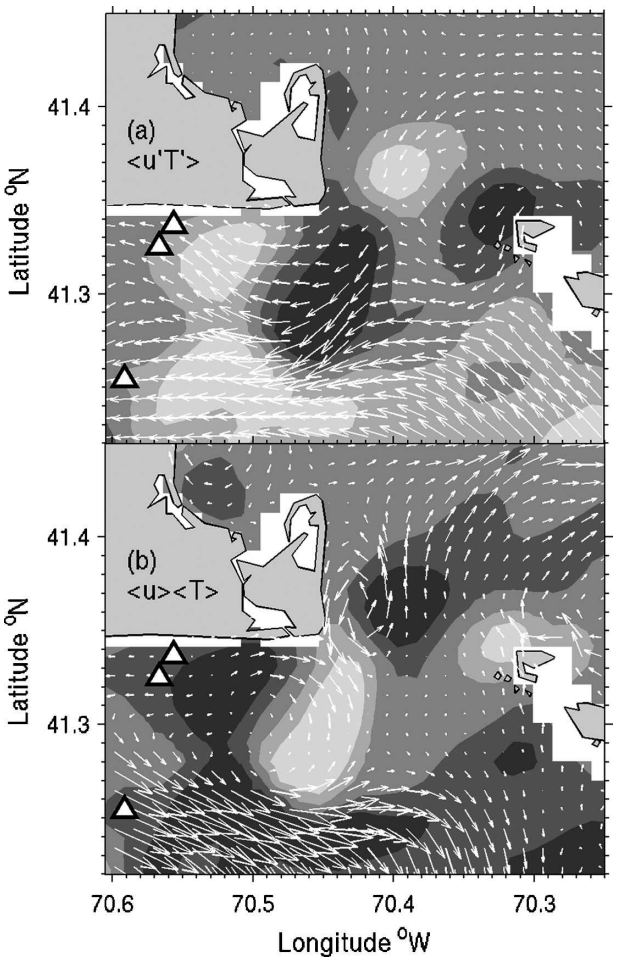

FIG. 13. (a) Depth-integrated eddy temperature flux $\langle \mathbf{u}'T' \rangle$ vectors in the Muskeget Channel region computed over 60 M_2 tidal periods during July. (b) Depth-integrated steady circulation temperature flux $\langle \mathbf{u} \rangle \langle T \rangle$ vectors. Shading shows the corresponding heat flux divergence. Dark areas are cooling; light areas are warming. Symbols mark (from south to north) the locations of mooring F, ASIT, and the MVCO node.

similar upwelling favorable wind event on 9 July also appears to cool the water column at mooring F but does not affect the modeled temperature at MVCO. A strong cooling event at MVCO occurs on 7 August during a period of northerly winds, but no corresponding cooling is seen at mooring F. It is conceivable that being less than 3 km from the coast, a strong offshore wind could cause cooling near to shore at MVCO without affecting the mooring F site an additional 9 km seaward. This disparity in response at MVCO and mooring F, and the short spatial scales evident in Fig. 13, illustrate that the dynamics affecting the depth-integrated heat budget are quite heterogeneous in this region.

The analysis presented here shows that lateral heat transport is significant near the MVCO site, with considerable spatial and temporal variability, and may need to be considered in the interpretation of heat balance observations at the MVCO Air–Sea Interaction Tower site.

6. Summary and conclusions

A modeling study of circulation on the inner shelf south of Cape Cod has been completed, with emphasis on the region in the environs of the Martha's Vineyard Coastal Observatory, for the time period of the CBLAST-Low field observations during the summer of 2002. The model was forced with surface meteorological conditions from a high-resolution COAMPS forecast, open boundary climatology, and tides. Tides prove important to the regional circulation, and an accurate tidal solution was achieved by using boundary harmonic constituents adjusted by assimilation of sea level data in a previous study (He and Wilkin 2006).

A series of idealized simulations compared the relative importance of the three principal drivers of regional circulation, namely, tides, winds, and the climatological mean inflow of waters from the Gulf of Maine. These studies showed that tides produce a strong anticyclonic circulation around the Nantucket Shoals. The net effect of open boundary inflows is in the same sense as the tides but generally confined to the outer shelf. Prevailing southwesterly winds during summer produce eastward flow through Nantucket Sound and moderate eastward flow south of Martha's Vineyard, but the latter is overwhelmed by the tidally driven circulation.

The model reproduces widely known features of the regional summer circulation: warm temperatures and weak eastward flow in Nantucket Sound, cool tidally mixed waters and an associated anticyclonic flow encircling the Nantucket Shoals, and strong stratification south of Martha's Vineyard. Comparisons with infrared satellite data and in situ observations from the 2002 CBLAST-Low field program show that the model simulates the dominant features of the evolution of the regional heat budget during summer 2002. Meteorological conditions in summer 2002 were similar to climatology over the past two decades, so conclusions from this study are expected to be representative of the region's typical summertime heat budget and circulation.

Lateral advection and submesoscale mixing of heat were largely unobserved by the CBLAST-Low observational network, so an objective of this study was to gauge the magnitude of horizontal heat transport in comparison with direct air–sea heat transfer in analyses of the vertical heat budget throughout the region. Three regimes emerge in the manner in which the sum-

mer heat budget evolves in the greater CBLAST-Low region. Nantucket Sound warms rapidly in early summer and then maintains warm temperatures with little net air–sea heating during the remainder of the season. On the Nantucket Shoals tidal mixing is sufficiently strong that the water column is well mixed in the vertical throughout the summer, thereby maintaining cool surface temperatures despite significant sustained surface heating. The extent of the well-mixed zone is consistent with the $\log_{10}(h/U^3)$ tidal mixing front criterion of Simpson and Hunter (1974). To the south of Martha's Vineyard and west of the Nantucket Shoals, the waters warm steadily throughout the summer in response to continued net air–sea heat flux with net advection playing a modest role in cooling the water column. In isolated areas the net heat advection is nearly zero, indicating an approximate one-dimensional vertical heat balance. One such area is immediately west of the southern extent of Nantucket Shoals where cool waters drawn out of the vertically mixed region undergo warming as they are transported rapidly northwestward.

Warm water exits Nantucket Sound through Muskeget Channel on every ebb tide, and these pulses migrate westward toward MVCO forming a bowl of warm water trapped against the south coast of Martha's Vineyard—a feature regularly observed in hydrographic sections. By separating the advective flux of temperature into mean and eddy contributions it is seen that the tidal pulsing produces a strong eddy heat flux emanating from Nantucket Sound that converges near MVCO, warming the water column. In contrast, the mean circulation acts to cool the region producing a net cooling in the environs of the observatory. There is considerable spatial variability in the magnitude of mean and eddy contributions to the heat balance because of the short spatial scales associated with the tidal eddies that dissipate as they encroach on MVCO. The general warming trend in the region south of Martha's Vineyard is occasionally arrested by abrupt cooling episodes associated with wind events.

It is concluded that lateral heat transport indeed plays a role in the heat budget throughout much of the CBLAST-Low observational area. Given the considerable spatial and temporal variability in the modeled heat transport dynamics in the vicinity of MVCO, the possibility that advection of temperature anomalies originating from the tidal pulses exiting Muskeget Channel, or from wind events, will need to be considered in the analysis and interpretation of vertically highly resolved observations of mixing and air–sea exchange from CBLAST-Low studies during 2002 and 2003 at the MVCO Air–Sea Interaction Tower site.

Acknowledgments. The research was funded by Office of Naval Research Grant N00014-04-1-0383. The CBLAST-Low program and ROMS development are also funded by ONR. Computational resources were provided by the DOD High Performance Computing Modernization Program. CBLAST mooring and CTD data were obtained by R. Weller, WHOI, with funding through ONR Grant N00014-05-10090. I am grateful to L. Hutto and J. Fredericks for providing CBLAST and MVCO data, S. Wang for the COAMPS meteorological forecasts, J. Bosch for satellite SST data, O. Schofield and J. Kerfoot for glider data, and J. Evans for help with model analysis. L. Lanerolle assisted with an earlier version of the model. T. Farrar, R. Weller, M. Pritchard, J. Edson, and J. Trowbridge offered many helpful discussions on the MVCO region dynamics. I thank two anonymous reviewers for constructive comments. Special thanks go to H. Arango for humoring many requests for new ROMS features, and R. He for fixing the tides. This paper is dedicated to the late David C. Chapman.

REFERENCES

Bigelow, H. B., 1927: Physical oceanography of the Gulf of Maine. *Bull. U.S. Bur. Fish.,* **40,** 511–1027.

Dinniman, M. S., J. M. Klinck, and J. W. O. Smith, 2003: Cross shelf exchange in a model of the Ross Sea circulation and biogeochemistry. *Deep-Sea Res. II,* **50,** 3103–3120.

Divins, D. L., and D. Metzger, cited 2003: NGDC Coastal Relief Model. National Geophysical Data Center. [Available online at http://www.ngdc.noaa.gov/mgg/coastal/coastal.html.]

Edson, J., and Coauthors, 2006: The Coupled Boundary Layers and Air–Sea Transfer Experiment in Low Winds (CBLAST-LOW). *Bull. Amer. Meteor. Soc.,* in press.

Eldridge, G., 2005: *Eldridge Tide and Pilot Book*. M. J. White, R. E. White, Jr., and L. F. White Publishers, 272 pp.

Fairall, C. W., E. F. Bradley, J. E. Hare, A. A. Grachev, and J. Edson, 2003: Bulk parameterization of air–sea fluxes: Updates and verification for the COARE algorithm. *J. Climate,* **16,** 571–591.

Flather, R. A., 1976: A tidal model of the northwest European continental shelf. *Mem. Soc. Roy. Sci. Liege, Ser. 6,* **10,** 141–164.

He, R., and J. L. Wilkin, 2006: Barotropic tides on the southeast New England shelf: A view from a hybrid data assimilative modeling approach. *J. Geophys. Res.*, **111,** C08002, doi:10.1029/2005JC003254.

Hodur, R. M., J. Pullen, J. Cummings, X. Hong, J. D. Doyle, P. J. Martin, and M. A. Rennick, 2002: The Coupled Ocean/Atmospheric Mesoscale Prediction System (COAMPS). *Oceanography,* **15,** 88–98.

Hutto, L., T. Farrar, and R. Weller, 2005: CBLAST 2003 Field Work Report. Woods Hole Oceanographic Institution, Tech. Rep. WHOI-2005-04, 136 pp.

——, J. Lord, P. Bouchard, R. Weller, and M. Pritchard, 2003: SecNav/CBLAST 2002 field experiment deployment/recovery cruises and data report, F/V Nobska, September 4 and 9, 2002, mooring data June 19–September 9, 2002. Woods

Hole Oceanographic Institution, Rep. WHOI-2003-07, 114 pp.

Lentz, S., K. Shearman, S. Anderson, A. Plueddemann, and J. Edson, 2003: Evolution of stratification over the New England shelf during the Coastal Mixing and Optics study, August 1996–June 1997. *J. Geophys. Res.,* **108,** 3008, doi:10.1029/2001JC001121.

Limeburner, R., and R. C. Beardsley, 1982: The seasonal hydrography and circulation over Nantucket Shoals. *J. Mar. Res.,* **40,** 371–406.

Linder, C. A., and G. Gawarkiewicz, 1998: A climatology of the shelfbreak front in the Middle Atlantic Bight. *J. Geophys. Res.,* **103,** 18 405–18 423.

Luettich, R. A., J. J. Westerink, and N. W. Scheffner, 1992: ADCIRC: An advanced three-dimensional circulation model for shelves, coasts, and estuaries. U.S. Army Engineer Waterways Experiment Station, Tech. Rep. DRP-92-6, 137 pp.

Lutjeharms, J. R. E., P. Penven, and C. Roy, 2003: Modelling the shear edge eddies of the southern Agulhas Current. *Cont. Shelf Res.,* **23,** 1099–1115.

MacCready, P., and W. R. Geyer, 2001: Estuarine salt flux through an isohaline surface. *J. Geophys. Res.,* **106,** 11 629–11 637.

Marchesiello, P., J. C. McWilliams, and A. F. Shchepetkin, 2001: Open boundary conditions for long-term integration of regional oceanic models. *Ocean Modell.,* **3,** 1–20.

——, ——, and ——, 2003: Equilibrium structure and dynamics of the California Current System. *J. Phys. Oceanogr.,* **33,** 753–783.

Mellor, G. L., and T. Yamada, 1982: Development of a turbulence closure model for geophysical fluid problems. *Rev. Geophys. Space Phys.,* **20,** 851–875.

Naimie, C. E., J. W. Loder, and D. R. Lynch, 1994: Seasonal variation of the three-dimensional residual circulation on Georges Bank. *J. Geophys. Res.,* **99,** 15 967–15 989.

Oke, P. R., and Coauthors, 2002: A modeling study of the three-dimensional continental shelf circulation off Oregon. Part I: Model–data comparisons. *J. Phys. Oceanogr.,* **32,** 1360–1382.

Peliz, Á., J. Dubert, D. B. Haidvogel, and B. Le Cann, 2003: Generation and unstable evolution of a density-driven eastern poleward current: The Iberian Poleward Current. *J. Geophys. Res.,* **108,** 3268, doi:10.1029/2002JC001443.

Pritchard, M., J. Gobat, W. Ostrom, J. Lord, P. Bouchard, and R. Weller, 2002: CBLAST-Low Pilot Study: Mooring deployment cruise and data report; FV Nobska, June 4 to August 17, 2001. Woods Hole Oceanographic Institution, Rep. WHOI-2002-03, 61 pp.

Shchepetkin, A. F., and J. C. McWilliams, 1998: Quasi-monotone advection schemes based on explicit locally adaptive diffusion. *Mon. Wea. Rev.,* **126,** 1541–1580.

——, and ——, 2003: A method for computing horizontal pressure-gradient force in an oceanic model with a non-aligned vertical coordinate. *J. Geophys. Res.,* **108,** 3090, doi:10.1029/2001JC001047.

——, and ——, 2005: The regional oceanic modeling system (ROMS): A split-explicit, free-surface, topography-following-coordinate oceanic model. *Ocean Modell.,* **9,** 347–404.

Simpson, J. H., and J. R. Hunter, 1974: Fronts in the Irish Sea. *Nature,* **250,** 404–406.

——, C. M. Allen, and N. C. G. Morris, 1978: Fronts on the continental shelf. *J. Geophys. Res.,* **83,** 4607–4614.

Wang, S., Q. Wang, Z. Gao, J. B. Edson, R. Weller, and C. Helmis, 2004: Evaluation of COAMPS real time forecast for CBLAST-Low summer experiments 2002/2003. Preprints, *16th Symp. on Boundary Layers and Turbulence,* Portland, ME, Amer. Meteor. Soc., CD-ROM, P8.2.

Warner, J. C., W. R. Geyer, and J. A. Lerczak, 2005: Numerical modeling of an estuary: A comprehensive skill assessment. *J. Geophys. Res.,* **110,** C05001, doi:10.1029/2004JC002691.

Wilkin, J. L., H. G. Arango, D. B. Haidvogel, C. S. Lichtenwalner, S. M. Glenn, and K. S. Hedström, 2005: A regional ocean modeling system for the long-term ecosystem observatory. *J. Geophys. Res.,* **110,** C06S91, doi:10.1029/2003JC002218.

Wilmott, C. J., 1981: On the validation of models. *Phys. Geogr.,* **2,** 184–194.